

# 3D cold pressure welded components – From the bonding mechanisms to the production of high strength joints

## 3D-Kaltfließpressgeschweißte-Bauteile - Von den Verbindungsmechanismen bis zur Herstellung hochfester Verbindungen

C. Gerlitzky<sup>1</sup>, C. Kuhn<sup>1</sup>, P. Groche<sup>1</sup>, T.H. Tran<sup>2</sup>, S. Zhang<sup>2</sup>, N.J. Peter<sup>2</sup>, M. Rohwerder<sup>2</sup>

In this work, a comprehensive analysis of the bonding mechanism involved in the formation of highly stable cold pressure welded aluminum-steel components is presented. After identification of relevant process steps to realize bonding the process is modified. Focusing on surface preparation methods, systematic manipulations are employed to identify the relevant parameters promoting the bond formation. The analysis is carried out by tensile stress testing of micro and macro samples as well as high resolution imaging of the joint zone. The results are enabling in a deeper understanding of the bonding mechanism.

**Keywords:** Cold pressure welding / surface treatment / bonding mechanism / surface contamination / multi-material bonds


In dieser Arbeit wird eine umfassende Analyse des Bindungsmechanismus, der an der Bildung von hochstabilen, kaltpressgeschweißten Aluminium-Stahl-Verbindungen beteiligt ist, vorgestellt. Nach dem Identifizieren relevanter Prozessschritte zur Realisierung eines Verbunds wird der Prozess modifiziert. Die Schwerpunkte der Untersuchungen liegen auf den Oberflächenpräparationsmethoden. Durch systematische Veränderungen werden die relevanten Parameter zur Ausbildung der Bindung identifiziert. Die Analyse erfolgt durch Zugspannungsprüfungen an Mikro- und Makroproben sowie durch hochauflösende Aufnahmen der Fügezone. Die Ergebnisse führen zu einem tieferen Verständnis des Bindungsmechanismus.

**Schlüsselwörter:** Kaltpressschweißen / Oberflächenpräparation / Verbindungsmechanismus / Oberflächenkontamination / Multi-Material-Verbindungen

<sup>1</sup> Technische Universität Darmstadt, Institute for Production Engineering and Forming Machines, Otto-Berndt-Straße 2, 64287 DARMSTADT, FEDERAL REPUBLIC OF GERMANY

<sup>2</sup> Max-Planck-Institut für Eisenforschung GmbH, Max-Planck-Straße 1, 40237 DÜSSELDORF, FEDERAL REPUBLIC OF GERMANY

64287 DARMSTADT, FEDERAL REPUBLIC OF GERMANY,  
E-Mail: gerlitzky@ptu.tu-darmstadt.de

 This is an open access article under the terms of the Creative Commons Attribution License, which permits use, distribution and reproduction in any medium, provided the original work is properly cited.

Corresponding author: C. Gerlitzky, Technische Universität Darmstadt, Institute for Production Engineering and Forming Machines, Otto-Berndt-Straße 2,

The copyright line for this article was changed on 13 November 2020 after original online publication and Projekt DEAL funding statement was added.

## 1 Introduction

Joining by forming or “conjoint forming” is a promising technology as the joining process is included in the forming process itself [1]. This type of forming processes can meet the current market demand for new and more complex multi material products. The process presented in this paper is a cold pressure welding extrusion process, where two billets of dissimilar materials are formed in the shape of a cup. The advantages of cold welding or solid state welding processes are the metallurgical strong bonds. In addition, the bond is free from intermetallic phases. Between certain material combinations, especially between the very relevant combination of steel and aluminum, these phases can be very brittle and therefore weaken the interface [2]. Therefore, they should be avoided and cold forming is the preferred bonding process.

## 2 State of the art

Cold pressure welding is an already commonly applied joining technology in roll bonding of electrical components in the automotive industry. It is a solid-state welding technology, where plastic deformation and high pressure is utilized in order achieve bonding. The process is divided into three phases [3]: In the beginning a contamination film and a brittle cover layer adheres to each joining partner. Plastic deformation causes a thinning of the contamination layer. The brittle surface layer breaks up and juvenile material is exposed. Due to normal stress initiated by the forming process, the

base material extrudes through the cracks and finally meets the other joining partner’s juvenile base material resulting in a solid bond [4, 5]. The model is extended by another step. It is stated, that before material closed bonding is achieved, aluminum reacts with the entrapped air and additional aluminum oxide forms [6]. However, the advantageous contact conditions during extrusion processes can be used to produce a material-closed bond between barely cold-weldable materials like steel and a commercial aluminum alloy [7, 8].

Previous dies about cold pressure welding show the importance of the contact conditions such as surface enlargement and normal pressure in the joint zone as well as surface treatments prior to the joining process itself. In this study, the influences of contact conditions in connection with the underlying bonding mechanism are analyzed by modifying the contact surface.

## 3 Materials and experimental details

The complete process chain of production from the material description to the final testing and characterization of the sample as well as the analysis methods are described in the following, *Figure 1*.

### 3.1 Materials

Steel 1.0401 billets (soft annealed and spheroidized) and aluminum alloy EN AW 6082 billets (artificially aged, T6) with a diameter of 41.5 mm and a thickness of 15 mm are employed as welding

**Figure 1.** Process chain of cold welding process including analyses methods.

materials [9]. This purpose of the heat treatment is to equalize the strengths of the two materials. The hardness of the aluminum after the heat treatment is 120 HV 2.5 and of the steel one is 150 HV 5. The adjustment is not absolutely necessary but is advantageous because the materials otherwise have dissimilar material flows during extrusion. A dissimilar material flow results in different flow velocities at the interface of the joint. This in turn leads to the shear and rupture of already joined areas [10]. The adjustment of the material flow can be achieved to a similar extent by slightly heating at least one of the materials directly before forming. However, deteriorating effects such as increased oxide formation must be taken into consideration in this case [11].

Prior to the cold welding process, the billets are further lubricated with a single bath lubricant. The kind of lubricant is particularly relevant because low viscosity lubricants are pressed into the joining gap in presence of high pressures during the forming process. This is why the solid lubricant (Gardomer L 6332, Chemetal) a lubricant specially designed for cold forming processes is used. The usage reduces high scatter in the resulting bond strength as the flow of the lubricant into the joint gap is avoided [9].

### 3.2 Experimental details

Joining surfaces of the metals to be welded are prepared by various surface treatments to analyze the influence of the surface roughness, residual stress state, contamination and chemical composition on the surface. To further analyze the bonding mechanism and especially the cracking of the surface layer, physical vapor deposition (PVD) layers are applied onto the contact surfaces. All surface treatments as well as the focus of the analysis are listed in tabular form, *Table 1*. Reference samples are ground at a P4000 grit. Brushed samples are prepared using a wire brushing process where short intense brushing resulted in the highest bond strength with process conditions documented [9]. Abrasive and ball peening are each performed for 2 minutes at 4 bar just within 10 minutes before the joining process. Each of these described processes is followed by a cleaning step with ethanol. A more intense surface cleaning is performed by etching.

**Table 1.** List of surface treatments including the investigation focus.

Name	Surface preparation	Focus
Ref	Reference-ground at P4000 grit	-
Brush	Wire brushed ! ethanol cleaned	Residual stresses, surface roughness
Peening	Abrasive or ball peening ! ethanol cleaned	
Ar-Plasma	Ground at P4000 grit ! Argon plasma treatment	Contamination
Etched-Fe	Ground at P4000 grit ! 2 min at 10 % Nital etchant	
Etched-Al	Ground at P4000 grit ! 2 min at 10 % Keller etchant	
PVD-Cr	Ground at P4000 grit ! Argon plasma treatment ! Chrome PVD layer application	Composition, Threshold of surface cracking
PVD-Ni	Ground at P4000 grit ! Argon plasma treatment ! nickel PVD layer application	
PVD-Ti	Ground at P4000 grit ! Argon plasma treatment ! titanium PVD layer application	

Oxide layers and contamination are removed by a two minutes lasting etching with either nitric acid - nital (steel) or Keller hydrofluoric acid etchant (aluminum). In order to remove organic contaminations a low-temperature plasma pretreatment of both welding surfaces (1.0401 and AA6082) with argon plasma is applied at a process gas flux of 80 sccm, while maintaining a pressure of 0.2 mbar for 30 min by using a custom-made plasma chamber [12]. The argon plasma pretreatment is initiated by the ignition of the plasma flame with a linear microwave source (Muegge GmbH, Germany) at a frequency of 2.4 GHz and a radio frequency power of 300 W [13]. To coat the samples PVD-Cr, PVD-Ni, PVD-Ti are transferred into a physical vapor deposition chamber (Leybold UNIVEX 450) after the plasma treatment. Deposition of 500 nm thick metal layers on both welding surfaces (1.0401 and AA6082) is carried out under high vacuum conditions. For this process titanium (99.99 %), nickel (99.99 %) and chromium (99.99 %) from the company Goodfellow are used. The idea of coating is not only to initiate the surface cracking at low sur-

face enlargements but also to visualize the cracking of the surface layer itself.

### 3.3 Production of joint with high bond strength and testing

For the forming operations, a direct driven servo motor press (Synchropress SWP 2500) with an extrusion tool is used [14]. The tool is designed in such a way that high surface enlargements and high contact normal pressures within the joint zone occur. The surface enlargement and normal pressure are analyzed by finite element analyses and increase during the forming process in general. However, each position along the weld has different contact conditions [10, 14]. After the surface treatments, samples were joint within less than 10 minutes as suggested and previously investigated [15]. The samples which were plasma treated and/or metal coated needed to be transported under vacuum. Within 10 minutes after being exposed to ambient air the samples are welded.

In order to evaluate the effect of different surface treatments on the bond strength, cross sections with a thickness of 3 mm are cut out of the cold pressure welded metal cups. Subsequently, either micro tensile test samples are extracted from the respective area using a wire eroding machine, or macro bond strength analysis is performed with a testing machine by Zwick & Roell (load cell 100 kN), *Figure 2a, b*. The micro tensile tests are performed by a testing machine from Kammrath & Weiss GmbH (load cell 5 kN). For each test con-

dition, six test specimens are analyzed with a test speed of 0.1 mm/s.

### 3.4 High resolution imaging methods

Investigations of the topography and the elemental composition of the cross section of the metal joint interface, the fracture surface and the cross section of the steel fracture surface after tensile tests are performed with a scanning electron microscope (Zeiss LEO 1550VP GEMINI) which is coupled to an energy dispersive x-ray (EDX) spectrometer (Oxford Instruments). Prior to the preparation of the cross section of the steel fracture surface nickel is electrodeposited on top as a protective layer. Cross sections are polished up to oxide particle suspension (OPS). For the analysis with the scanning transmission electron microscope (STEM), a FEI Helios 600 Nanolab focused ion beam (FIB) is used to prepare a electro transparent transmission electron microscope lamella from the metal joint interface. Scanning transmission electron microscopy is performed on a Fei Titan Themis microscope operated at 300 kV. Scanning transmission electron microscopy - high angle annular dark field (HAADF) images are recorded with the detector collecting semi angles between 73 mrad and 352 mrad. Energy dispersive x-ray spectrum imaging is recorded using a windowless, four quadrant silicon-drift detector (Super-X) with a solid angle of more than 0.7 sr. Electron energy loss spectroscopy (EELS) spectrum imaging is acquired using a Quantum ERS energy filter configured in the image-coupled mode with a 35 mrad collection semi angle. Multi-

**Figure 2.** a) Cross section of a cold press welded metal joint indicating the micro tensile test specimen extraction sides P1 and P2 and b) the geometry of macro tensile specimens with clamping regions during testing and c) resulting bond strength measurements with standard deviation as error bar.

variate analysis on energy dispersive x-ray and electron energy loss spectroscopy spectrum imaging data is performed to reduce the noise and to identify features in the datasets [16].

## 4 Results and discussion

The resulting bond strength measurements of each test type are summarized in a diagram, Figure 2c. The results obtained with the macro method are compared with the averaged results using micro test specimen. If the bond strengths along the weld (represented by the micro measurements at P1 and P2) are similar the micro and the macro method yield the same bond strength within the accuracy of the measurement. This is the case for the titanium coated samples. If, however the bond strengths at P1 and P2 are significantly different, as for the chromium coated samples, the macro method yields significantly lower bond strengths than the micro method. This behavior indicates different failure mechanism in the macro tensile tests: titanium coated samples show a brittle fracture along the welded, whereas area chromium coated samples fail successively along the joint. In the latter case local variations of the bond strength are relevant. Those

can only be measured using micro tensile specimens.

The bond strengths of the samples with regard to the influence of residual stresses and surface roughness show that peened samples could not be joined. The brushed samples are significantly better but do not reach the strength of the reference sample *Figure 3a*. Pretest show no significant influence of surface brushing onto the steel as the roughness stays between  $5.3\ \mu\text{m}$  and  $6.7\ \mu\text{m}$  and the residual stresses at  $246\ \pm\ 5\ \text{MPa}$ . Therefore, the focus of the surface variation lies on the aluminum side. The reference sample has compressive residual stresses of  $115.5\ \text{MPa}$  at the surface, which can be reduced to  $29.3\ \text{MPa}$  by brushing measured by x-ray diffraction [9]. The highest bond strength is however achieved when the brushing process is adapted and results in compressive residual stresses of  $60\ \text{MPa}$  [9]. The highest compressive residual stresses for this experimental series are measured for ball peening preparation with  $420\ \text{MPa}$  (measured by hole drilling method) [14]. Note that the results of the discussed measurements cannot be attributed to residual stresses alone since the surface contamination of the samples was not analyzed. Further investigations should be performed to validate to which extend the ball peening process does re-

**Figure 3.** Macro tensile test bond strength analysis in dependency of a) surface roughness and residual stresses, b) contamination c) composition and threshold of surface cracking d) intermediate layer under the SEM and e) contamination measured [15] f) contaminated (black) and corroded (dark grey) steel (light grey) surface of etched-Fe under SEM.

duce the surface contamination. In this study, analyses with definable contaminations are performed as it is more likely that the residual stresses have no significant influence within the varied parameter set since residual stresses induced by forming are significantly higher than any stress achievable by a surface preparation used in these experiments.

The roughness is measured by confocal white light microscopy ( $\mu$ Surf<sup>®</sup>, Keyence) and adjusted for different brushed samples between 0.5  $\mu\text{m}$  and 22  $\mu\text{m}$ , but it cannot be related to the resulting bond strength [9]. Only the surface structure is noted to be relevant, as certain smeared structures form an interlayer, which separates the ground materials from each other during the joining process itself [9]. This behavior is also found for the abrasive peened samples which did not show any measurable bond strength but significant amount of adhesions on the steel fracture surface after tensile testing. The structure with sharp peaks leads to an intermediate layer [14], Figure 3d. In any case, brushing shows a clear trend for increased bond strength if short but strong brushing is performed [9]. Further analysis with a stronger brushing machine might lead to an additional increase of bond strength resulting in a failure of the weaker base material [14].

In conclusion, it is not the surface roughness but the surface structure that is more relevant. If the surface shows many sharp, thin peaks before the forming this surface structure collapses under the load of the punch and forms an interlayer. This inhibits the bonding of juvenile ground material as it separates the joining partners.

The bond strength results show the influence of more contaminated samples (e.g. etched-Fe) in comparison to the samples with little surface contamination, Figure 3b. Extensive analysis showed that by reducing the organic contamination, scatter in the bond strength can be decreased as well as the bond strength increased [13]. The reduction of the organic contamination is represented by the carbon amount (C1s), Figure 3e. Further analyses are performed with etching the steel or aluminum joining partner, which does not only reduce the organic contamination but also the oxide layer thickness. Etching the aluminum alloy results in even higher bond strengths, which is in good accordance with the published results [14]. On the contrary, etching the steel side leads to extremely high scatter and

low bond strengths. The reason for this phenomenon is found on the surface of the steel sample of the macro tensile tested samples, where corrosion of the steel is detected, Figure 3f. Hence, etching both joining partners at the same time also causes low bond strengths due to the corrosion of the steel. Altogether, surface contamination is an extremely relevant parameter. It is more relevant than the surface roughness as even a perfectly rough structure cannot be joined if corrosion products, lubricant or organic residuals are to be found between the joining partners. However, the resulting oxide thickness on the etched aluminum samples cannot be measured by the means of x-ray photoelectron spectroscopy (XPS) as the surface roughness is too high. Nevertheless, the bond strengths indicate that the decrease of brittle oxide layer leads to an even stronger joint, Figure 3b.

Composition of the surface and threshold of surface cracking during forming is crucial for bonding and the resulting bond strength. This is further investigated by experiments with metal coated samples. However, results of the bond strength do not reveal remarkable differences, Figure 3c. Thus, deeper examinations with high resolution methods are performed.

First, the cross sections of the metal interlayer joints show that instead of a thinning-out behavior a considerable break-up of the physical vapor deposited metal interlayers to smaller “islands” occurs during the cold pressure welding process, while the initial thickness of the individual interlayers (approx. 500 nm) remains almost unchanged, Figure 4b-c. However, for individual cases a different pronounced thinning-out or rounding-off can be observed at the edges of the fragmented interlayers. Within the space between the interlayer islands, a predominant infiltration of aluminum can be observed, which does not apply for all interlayer gaps. The edges of the islands seem to preferentially promote the local flow and this evokes the surface enlargement of the aluminum substrate into the gaps, while a flow of steel is not evident, Figure 4b. The fragmentation of the deposited interlayers leads to an exposure of new juvenile interlayer surfaces at the break-up area, which can eventually contribute to increased bond strength in conjunction with the locally promoted surface enlargement of aluminum.

A closer look at the steel and aluminum fracture surfaces of the corresponding titanium or chromium

**Figure 4.** SEM micrographs displaying the cross section of the reference and PVD metal interlayer joint (a-c) and the corresponding top view on the Fe (d-f) and Al (g-i) fracture surface after tensile tests.

physical vapor deposited metal joints after tensile tests shows that both fracture surfaces exhibit a honey-comb like structure with interlayer island plates between aluminum protrusions of varying magnitude, Figure 4e, f, h, i. Aluminum protrusions and interlayer island plates on the aluminum and steel fracture surface suggest two major types of material failure: A predominantly cohesive failure in the aluminum bulk material and an adhesive failure either between the deposited metal  $j$  metal interlayer (here: Ti  $j$  Ti or Cr  $j$  Cr) or between the deposited metal interlayer  $j$  substrate.

In order to define at which point the brittle adhesive failure can occur, cross sections of the steel fracture surface specimen after tensile test of the Ti-PVD metal joint are analyzed, Figure 5. Analysis of the steel fracture surface interface indicates a predominant ductile failure in the Al bulk or brittle failure between the Ti  $j$  Ti interlayer. The aluminum protrusions seem to have direct contact with the steel substrate suggesting mainly the extrusion

of the aluminum material through the torn-up interlayers onto the steel substrate. Additionally, the cross section of the steel fracture surface shows that within the aluminum protrusions titanium interlayers can also be entrapped, Figure 5b. The infiltration and extrusion of aluminum within and along the interlayer edges onto the steel substrate are further investigated with scanning transmission electron microscopy imaging and spectroscopy (EDX, electron energy loss spectroscopy), Figure 6. A clearer deformation and rounding-off of the interlayers at the edges can be observed as compared to the scanning electron microscope (SEM) investigations of the cross sections, Figure 5b. The aluminum material flows along the torn-up interlayer edges without any noteworthy gaps, Figure 6a. From the energy-dispersive x-ray spectroscopy mapping, a highly thinned-out titanium interlayer area becomes evident, which extends from the aforementioned area at the Fe  $j$  Ti  $j$  Al intersection upwards, Figure 6b. The titanium inter-

**Figure 5.** Cross section of the steel fracture surface after tensile tests of Ti-PVD metal joint.

**Figure 6.** STEM-HAADF image of the Ti-PVD metal joint at the welding interface (a) and the corresponding EDX maps (b) and EELS maps at bond interface with a continuous layer of titanium (pixel size: 2 nm) (c1) and discontinuous layer of titanium (pixel size: 1 nm) (c2). The numerical markers indicate the recording area of the EELS maps.

layer is studied at higher resolution by electron energy loss spectroscopy that shows a discontinuous layer of up to 10 nm width, Figure 6c. Thus, apart of the surface enlargement of aluminum and steel, also a considerable surface enlargement of titanium can take place during the cold pressure welding process. This might also conclude with the findings of other researchers who find aluminum oxides which are supposed to be newly formed by entrapped air [6]. We suggest that this can also be strongly thinned out surface oxide from the beginning of the process.

This finding means in our case, that a direct contact between juvenile titanium bulk material

with juvenile bulk material of aluminum and steel is possible. This is not visible in the scanning electron microscope, Figures 4, 5. Hence, a failure in the aluminum bulk material can be the result of a stronger bond strength either at the Al j Fe or the Al j Ti interface (if thinned out). Though, the inter-layer islands do not exhibit any noticeable thinning out or surface enlargement. Consequently, it can be stated that the physical vapor deposition onto the welding surfaces of the steel and aluminum prior to the cold pressure welding process do not contribute to an increased bond strength. This can be underlined with the results derived in micro tensile tests, where the reference sample resulted in an averaged



bond strength of the micro tensile tests of 259.8–20.5 MPa and the Ti-PVD sample 272.68–23.30 MPa.

In any case, a different cracking behavior and therefore initiation of the welding process can be visualized. This is confirmed by additional experiments analyzing different forming states, *Figure 7a*. The PVD-Ti and PVD-Ni layer result in the same bond strength in the final forming state. However, 6 mm before the bottom dead center is reached the PVD-Ti samples show significantly higher bond strength, *Figure 7b*. Every forming state can be correlated to a specific normal pressure and surface expansion using finite element simulations of the process, *Figure 7c*. These were calculated using DEFORM 2D/3D as described in [10]. The surface expansion is significantly lower at the forming state 6 mm before the bottom dead center. Thus the bonding is initiated at lower surface enlargements for the Ti-PVD samples compared to the Ni-PVD samples. The contact normal pressure does not affect these results since it is similar for the compared forming states.

Summarized the bonding mechanism is described by the following steps:

1. Since pressure welding takes place under atmospheric conditions there are oxides on the joining surfaces of both joining partners even after appropriate surface treatment [3].
2. During forming, the punch force leads to an increase in contact normal stresses along the joining zone [3].
3. The plastic deformation leads to local surface enlargements and thus to the breaking up of the oxide layers on the surface layers [3]. These oxide layers undergo a brittle crack but could also thin out similar to the behavior of other metal layers as shown here for titanium.
4. The continuous normal contact stress causes the aluminum to be extruded through the cracks in the oxides to the base material as the less strong material of the join pair. However, resulting form-closed bonds between aluminum and the cracks of for instance the titanium interlayer does not significantly increase the bond strength.
5. Bond strength results show that the surface treatment of the steel side is not relevant if it is contamination free, which confirms the suggested mechanism of the last step where iron ions of the iron oxide react with the metallic aluminum. This reduces the iron to elemental iron, which forms a covalent bond with the metallic aluminum.

This leads to the result that the Al-Fe bonds which are formed between juvenile material are most likely the key points. Strengthening the bond strength by an optimized interlayer as for example nickel or titanium is not beneficial.

**Figure 7.** Bond strengths (b) in dependence on forming states (a) with corresponding contact normal pressure and surface expansion obtained by finite element (FE) simulation (c).

## 5 Conclusions

The surface treatments performed are employed to lead to a deeper understanding of the bonding mechanism as well as the effect considering their different level of impact on the resulting bond strength.

Due to the comparison to literature and findings within the presented experiments the following sequence from least important to most important is suggested:

1. Residual stresses – This is the least relevant parameter as we assume it is overcome by the normal pressure at the very beginning of the forming process.
2. Composition – The bonding of one joining partner to an applied metal layer does not contribute to the resulting bond strength as the achieved bonds between juvenile materials are the strongest. The joints between steel and aluminum are in addition the most frequent ones contributing to the bond strength.
3. Surface roughness – Bond strength is achieved by material closed bonding, not mechanical closed bonding. The surface structure, however, should be considered as it can inhibit the bonding by forming an intermediate layer.
4. Threshold of surface cracking – If the surface expansion and therefore the overall ratio from initial to final surface is the same, only very few percentages in bond strength can be optimized. The different threshold of surface cracking and different number of cracks only results in a different amount of form closed bonding which is significantly less strong than the achieved material closed bond.
5. Contamination – The contamination can inhibit the bonding completely as it stretches out during the forming process and reduces the amount of bondable surface not covered by any contamination by exposing the juvenile material.

Concluding it is demonstrated that if all the above mentioned parameters are considered and the process is designed to prevent relative movement of the materials, high contact normal pressure exist during forming and a significant surface enlargement are existent, the bond strength cannot be further enhanced than up to the strength of the aluminum.

However, it is still questionable, what is the governing mechanism on atomic level which results to these high bond strengths. In further studies the bonding mechanism between aluminum and iron will be investigated.

## Acknowledgements

The authors acknowledge the DFG (Deutsche Forschungsgemeinschaft) for funding via the sub-projects ER 601/3-1, ER 601/3-2, GR 1818/48 1-3 and RO 2027/9-3, within the priority program 1640 “Joining by plastic deformation”. As well we would like to thank A. Erbe, S. Wohletz, A. Altin, W. Krieger, S. Volz, B. Niessen, A. Franceschi and T. Preuschoff for the fruitful discussion and support during the six years of research on this project. Open access funding enabled and organized by Projekt DEAL.

## 6 References

- [1] P. Groche, S. Wohletz, A. Mann, M. Krech, V. Monnerjahn, *IOP Conf. Ser.: Mater. Sci. Eng.* **2016**, *119*, 012025.
- [2] M. Zamanzade, A. Barnoush, C. Motz, *Crytals* **2016**, *6*, 10.
- [3] N. Bay, C. Clemensen, O. Juelstorp, T. Wanheim, *CIRP Ann.* **1985**, *34*, 221.
- [4] N. Bay, *J. Eng. Ind.* **1979**, *101*, 121.
- [5] N. Bay, *Proceed. Instn. Metall. Spring Res. Conf.* **1981**, *47*.
- [6] D.R. Cooper, J.M. Allwood, *J. Mater. Process. Technol.* **2014**, *214*, 2576.
- [7] P. Groche, S. Wohletz, M. Brenneis, C. Pabst, F. Resch, *J. Mater. Process. Technol.* **2014**, *214*, 1972.
- [8] Y. Yoshida, T. Matsubara, K. Yasui, T. Ishikawa, T. Sukanuma, *Key Eng. Mater.* **2012**, *504*, 387.
- [9] C. Gerlitzky, S. Volz, P. Groche, *Key Eng. Mater.* **2018**, *767*, 309.
- [10] C. Gerlitzky, S.M. Arbo, I. Westermann, P. Groche, presented at *ESAFORM*, Mondragon, Spain, 08. May – 10. May, **2019**, 117.
- [11] P. Groche, S. Wohletz, A. Erbe, A. Altin, *J. Mater. Process. Technol.* **2014**, *240*, 2040.

- [12] J. Raacke, M. Giza, G. Grundmeier, *Surf. Coat. Technol.* **2005**, *200*, 280.
- [13] T.H. Tran, C. Gerlitzky, M. Rohwerder, P. Groche presented at *ESAFORM*, Mondragon, Spain, 08. May – 10. May **2019**, 116.
- [14] S. Wohletz, *Ph.D. Thesis*, TU Darmstadt, Germany, **2017**.
- [15] R. Jamaati, M.R. Toroghinejad, *Mater. Sci. Eng.* **2010**, *527*, 2320.
- [16] S. Zhang, C. Scheu, *Microscopy* **2018**, *67*, 133.

Received in final form: June 18<sup>th</sup> 2019